

Electron and Proton Energy Loss via Rovibrational Excitation of Molecular Hydrogen in Fusion Detached Plasmas^{*)}

Keiji SAWADA

Faculty of Engineering, Shinshu University, 4-17-1 Wakasato, Nagano 380-8553, Japan

(Received 10 January 2022 / Accepted 28 February 2022)

Electron and proton energy-loss rate coefficients in a fusion detached plasma, formed through collisions with molecular hydrogen, are investigated using a rovibrationally resolved collisional-radiative model of molecular hydrogen [K. Sawada and M. Goto, *Atoms* **4**, 29 (2016)]. The rovibrational population distribution of $X^1\Sigma_g^+$ in electrons and protons, both with a temperature of 1 eV and density of 10^{16} cm^{-3} , is solved time-dependently with an initial 300 K Boltzmann distribution. Energy loss of electrons by rovibrational excitation in $X^1\Sigma_g^+$ is approximately one or two orders of magnitude larger than that by excitation to the triplet $b^3\Sigma_u^+$ state.

© 2022 The Japan Society of Plasma Science and Nuclear Fusion Research

Keywords: collisional-radiative model, molecular hydrogen, rate coefficient, vibrational, rotational, detached plasma, molecular assisted recombination

DOI: 10.1585/pfr.17.2403044

1. Introduction

Reaction rate coefficients of molecular hydrogen processes in detached divertor plasmas are very sensitive to the initial rovibrational state [1]. The dissociative attachment process, the first step of well-known molecular assisted recombination (MAR) [2], is one of these processes. In modeling divertor plasmas, evaluating the rovibrational population distribution of molecular hydrogen is essential.

We have constructed a rovibrationally resolved collisional-radiative model of molecular hydrogen to evaluate the population distribution. The numbers of 4133 rovibrational states in electronic states up to $n = 6$, where n is the united atom principal quantum number, are considered. We calculated the effective reaction rate coefficients of molecular processes due to the impacts of electrons, protons, neutral atoms, and molecules in a fusion detached divertor plasma [1].

The rovibrational excitation by the plasma particles may affect the energy balance of low-temperature detached divertor plasmas. However, they are not considered in widely-used codes. In this study, using the rovibrational collisional-radiative model of the hydrogen molecule, we evaluate effective energy-loss rate coefficients of the electrons and protons through molecular impact processes in a type of plasma with detached plasma parameters.

Many hydrogen molecules in fusion plasmas originate from release from walls. Molecules released from various wall positions experience rovibrational excitation in the plasma and produce a population distribution at each position in a plasma. For simplicity, in this paper, we calculate the time-dependent rovibrational population in a uniform

plasma, with an initial 300 K Boltzmann distribution.

2. Collisional-Radiative Model of H_2

We apply the model developed in Ref. [1] to the present energy loss calculation. Table 1 lists the processes in the code. For cross-section data and transition probability data, see Ref. [1]. We use plasma parameters which are obtained from a detached plasma simulation of SlimCS DEMO [3,4]. The temperatures of the electron, T_e , proton, T_i , and atomic hydrogen, T_H , are all 1 eV. The densities of both the electrons and protons are 10^{16} cm^{-3} and the density of atomic hydrogens is 10^{15} cm^{-3} .

Figure 1 shows some of the rovibrational energies and wave functions of $X^1\Sigma_g^+$ calculated from the Schrödinger equation [1]. Plasma particles with kinetic energy larger than the energy differences in levels in Fig. 1 excite molecules rovibrationally.

The number of 301 rovibrational population distribution of the $X^1\Sigma_g^+$ is solved time-dependently. An initial 300 K Boltzmann distribution population is given at $t = 0$ s, as shown in Fig. 2. This may be able to be taken as gas puffed molecules. The initial total molecular density is 1 cm^{-3} . The quasi-steady-state solution [5,6] is applied to the rovibrational states in the electronic excited states.

3. Results

Figures 3(a) and 3(b) show examples of the calculated rotational population distribution in the $H_2(X^1\Sigma_g^+)$ as a function of time. Figure 4 shows the time-dependent effective rate coefficients for MAR (P5–P7) and (P9–P12) in Table 1 and the total molecular density calculated from the obtained rovibrational population density. Figure 4 also shows the effective rate coefficients of the production of

author's e-mail: ksawada@shinshu-u.ac.jp

^{*)} This article is based on the presentation at the 30th International Toki Conference on Plasma and Fusion Research (ITC30).

Table 1 Molecular processes included in the present model. p is the principal quantum number of H atom. H_2^* denotes electronically excited molecule.

Label	Process
(P1)	$H_2(X^1\Sigma_g^+, v) + e \rightarrow H_2(b^3\Sigma_u^+) + e \rightarrow H + H$
(P2)	$H_2(X^1\Sigma_g^+) + e \rightarrow H + H(p \geq 2) + e$
(P3)	$H(p \geq 2) \rightarrow H^* \rightarrow H$
(P4)	$\rightarrow H^+ + e$
(P5)	$H_2(X^1\Sigma_g^+, v, J) + e \rightarrow H_2^- \rightarrow H(p = 1 \text{ or } 2) + H^-$
(P6)	$H^- + H^+ \rightarrow H + H(p = 2 \text{ or } 3)$
(P7)	$H(p = 2 \text{ or } 3) \rightarrow H^* \rightarrow H$
(P8)	$\rightarrow H^+ + e$
(P9)	$H_2(X^1\Sigma_g^+, v) + H^+ \rightarrow H_2^+(X^2\Sigma_g^+, v') \rightarrow H$
(P10)	$H_2^+(X^2\Sigma_g^+, v') + e \rightarrow H_2^+(X^2\Sigma_g^+, v'') + e$
(P11)	$H_2^+(X^2\Sigma_g^+, v'') + e \rightarrow H + H(p \geq 2)$
(P12)	$H(p \geq 2) \rightarrow H^* \rightarrow H$
(P13)	$\rightarrow H^+ + e$
(P14)	$H_2(X^1\Sigma_g^+, v, J) + e \leftrightarrow H_2^*(\text{excited}, v', J') + e$
(P15)	$H_2^*(\text{singlet}, v, J) \rightarrow H_2(X^1\Sigma_g^+) + h\nu \rightarrow H + H$
(P16)	$H_2^*(\text{triplet}, v, J) \rightarrow H_2(b^3\Sigma_u^+) + h\nu \rightarrow H + H$
(P17)	$H_2^*(\text{excited}, v, J) + e \rightarrow H_2^+(X^2\Sigma_g^+, v') + 2e$
(P18)	$H_2^*(\text{excited}, v, J) \rightarrow H_2(X^1\Sigma_g^+, v', J') + h\nu$
(P19)	$H_2(X^1\Sigma_g^+, v, J) + e \leftrightarrow H_2(X^1\Sigma_g^+, v', J') + e$
(P20)	$H_2(X^1\Sigma_g^+, v, J) + H^+ \leftrightarrow H_2(X^1\Sigma_g^+, v', J') + H^+$
(P21)	$H_2(X^1\Sigma_g^+, v, J) + H \leftrightarrow H_2(X^1\Sigma_g^+, v', J') + H$
(P22)	$H_2(X^1\Sigma_g^+, v) + H \rightarrow H + H + H$
(P23)	$H_2(X^1\Sigma_g^+, v, J) + e \rightarrow H_2^+(X^2\Sigma_g^+, v') + 2e$
(P24)	$H_2(X^1\Sigma_g^+, v, J) + e \rightarrow H^+ + H + 2e$
(P25)	$H_2^+(X^2\Sigma_g^+, v) + e \rightarrow H + H^+ + e$

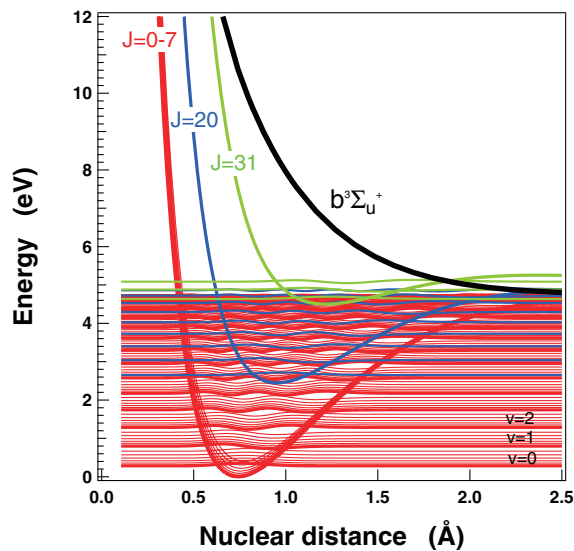


Fig. 1 Potentials of $X^1\Sigma_g^+$ ($J = 0-7, 20, 31$) and $b^3\Sigma_u^+$, and vibrational energy levels for $X^1\Sigma_g^+(v, J = 0-7, 20, 31)$ are shown. The vibrational wave function is superimposed on the energy level lines.

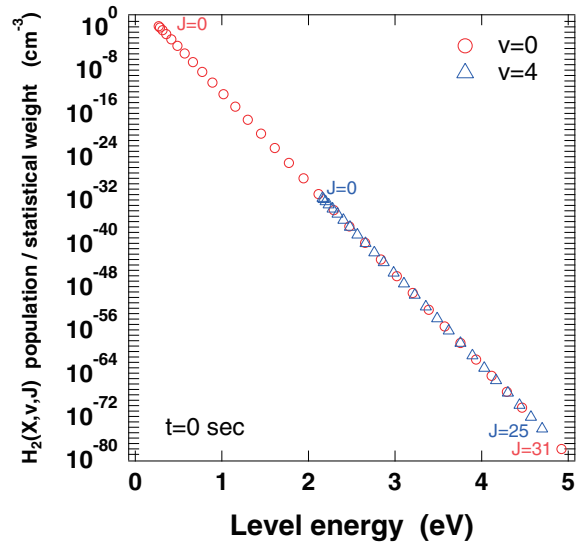


Fig. 2 Initial 300 K rovibrational population distribution divided by the statistical weight of the rotational states. As examples, those for $X^1\Sigma_g^+(v = 0, J)$ and $X^1\Sigma_g^+(v = 4, J)$ are shown.

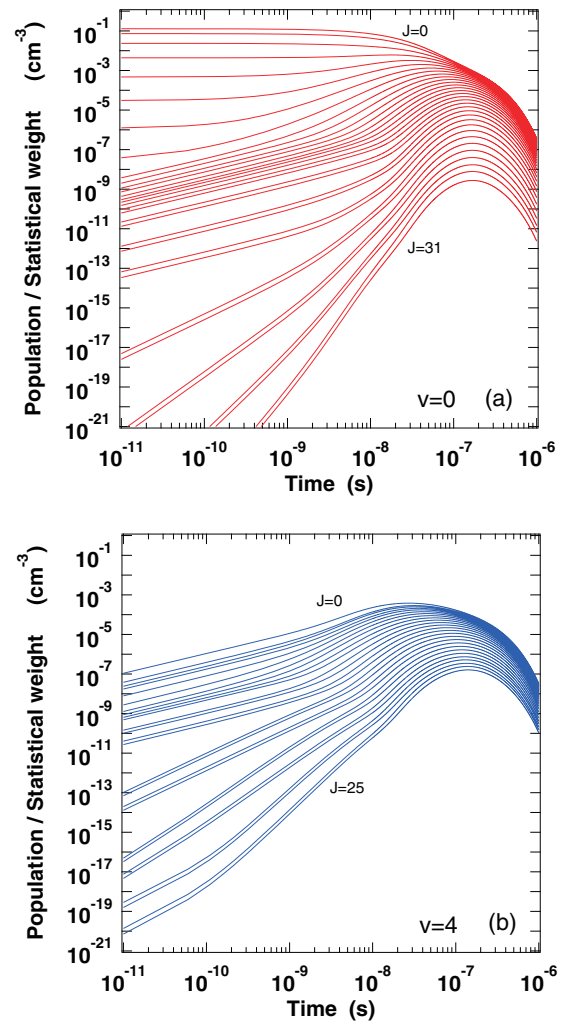


Fig. 3 Population divided by the statistical weight of the rotational states in (a) $X^1\Sigma_g^+(v = 0)$ and (b) $X^1\Sigma_g^+(v = 4)$.

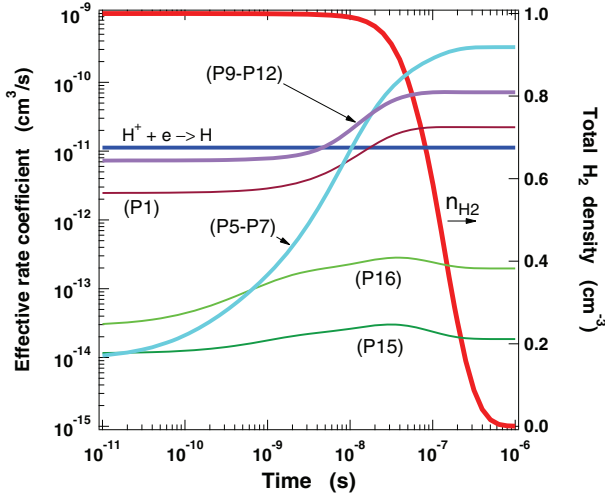


Fig. 4 Time-dependent total molecular density (right axis) and $P_{H_2}^H$ in Eq. (1) (left axis). The values for (P1), (P15), and (P16) should be multiplied by two because two atoms are produced.

atomic hydrogen from H_2 , $P_{H_2}^H$, by the other processes. The definition of the effective rate coefficient for each process is

$$\frac{dn_H}{dt} = P_{H_2}^H n_{H_2} n_e, \quad (1)$$

where n_e is the electron density, and n_{H_2} is the total population density of H_2 .

We calculate the energy-loss rate coefficients of (P19), (P20), and (P21) processes, shown in Table 1. The energy loss rate coefficient, L_k , is defined for each process as,

$$\frac{dE_k}{dt} = L_k n_{H_2} n_k, \quad (2)$$

where k denotes electron, proton or atomic hydrogen, E_k denotes energy per unit volume of k particles, and n_{H_2} and n_k are the density of the hydrogen molecules and the k particles, respectively. The energy-loss rate coefficient, L_k , is given as,

$$L_k = \frac{\sum_{i,j} R_k(i,j) n_{H_2}(i) (E_j - E_i)}{\sum_i n_{H_2}(i)}, \quad (3)$$

where $R_k(i,j)$ is the transition rate coefficient from i state to j state by k particles, $n_{H_2}(i)$ is the population of state i , and $E_j - E_i$ is the energy difference. L_k changes with the rovibrational population distribution in $H_2(X^1\Sigma_g^+, v, J)$.

Figure 5 shows the effective energy-loss rate coefficients as a function of time. The changes of these values result from the increase of the excited rovibrational population in the $X^1\Sigma_g^+$.

For comparison, we calculate the energy-loss rate coefficients of well-known processes of (P1) and (P23) from Table 1. Figure 5 shows these rate coefficients. We obtained the energy-loss distribution in process (P1) by calculating the Franck-Condon factor (FCF) between the vibrational wave function in the $X^1\Sigma_g^+$ and the $b^3\Sigma_u^+$ continuum vibrational wave function. The increase with time in

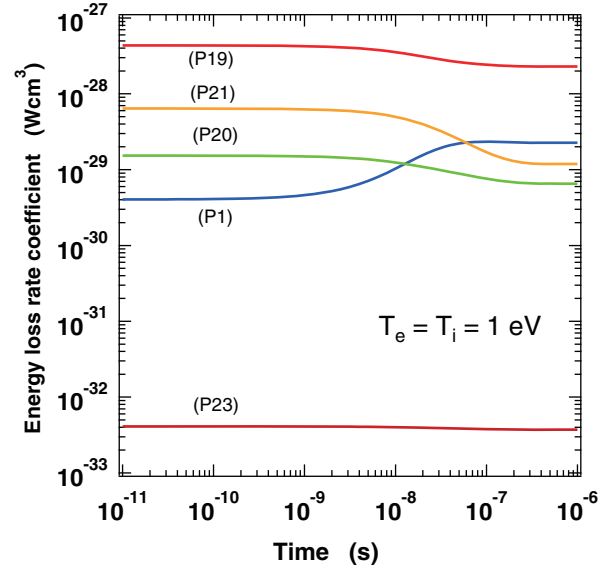


Fig. 5 Effective energy loss rate coefficients, L_k , defined in Eq. (3).

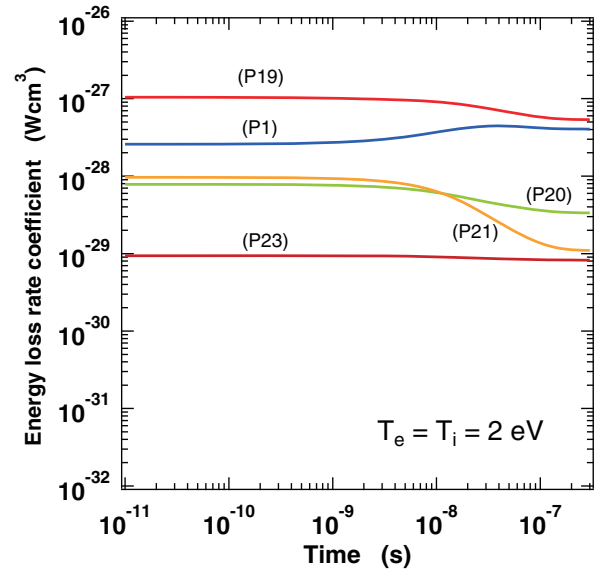


Fig. 6 Effective energy loss rate coefficients, L_k , defined in Eq. (3). $T_e = T_i = 2$ eV.

(P1) results from the rise of the excitation rate coefficient for upper rovibrational states [7]. Energy loss of electrons by rovibrational excitation in $X^1\Sigma_g^+$ is approximately one or two orders of magnitude larger than that by (P1).

Figure 6 shows another calculation where $T_e = T_i = 2$ eV. The other parameters in this calculation are the same as those described earlier. The energy loss by rovibrational excitation becomes dominant for plasmas whose temperature is lower than 2 eV.

4. Conclusion

The rovibrationally resolved H_2 collisional-radiative

model was applied to evaluate the energy loss of electrons and protons through collision with H_2 in plasmas. We solved the time-dependent rovibrational population distribution of $X^1\Sigma_g^+$. In the increase of the excited rovibrational population, the rovibrational excitation always dominates the energy loss of the plasma. The result here suggests this energy loss will be essential for low-temperature detached plasmas regardless of the initial rovibrational distribution at the wall.

As far as we know, traditional neutral transport codes for fusion plasmas do not include energy loss by rovibrational excitation. Negligence of rovibrational excitation may lead to underestimating the plasma energy loss and overestimating the plasma temperature and heat flux to divertor plates. This study indicates that rovibrational states in $X^1\Sigma_g^+$ should be tracked as independent species in neutral transport codes to calculate the rovibrational population distribution. As for this, we have already integrated the present collisional-radiative model into our neutral transport code and applied it to an ionizing plasma of the large helical device (LHD) [8]. We have also calculated the rovibrational population distribution at all plasma positions by providing the spatial electron temperature and density distributions. The initial rovibrational states and velocity of molecules released from a graphite divertor target have been provided by MD simulation [9]. We will apply this integrated code to detached recombining plasmas to further evaluate energy loss of plasma particles.

Acknowledgments

The research was partially supported by Grant-in-Aid for Scientific Research (C) No.18K03581, 19K03800, 19K03802 and (A) 20H00138 from the Japan Society for the Promotion of Science, and by the NIFS Collaborative Research Program NIFS16KOAP031.

- [1] K. Sawada and M. Goto, *Atoms* **4**, 29 (2016).
- [2] S.I. Krasheninnikov, A. Yu. Pigarov and D.J. Sigmar, *Phys. Lett. A* **214**, 285 (1996).
- [3] K. Hoshino, K. Shimizu, N. Asakura, T. Takizuka, M. Nakamura and K. Tobita, *Contrib. Plasma Phys.* **52**, 550 (2012).
- [4] K. Hoshino, K. Sawada, R. Idei, S. Tokunaga, N. Asakura, K. Shimizu and N. Ohno, *Contrib. Plasma Phys.* **56**, 657 (2016).
- [5] K. Sawada and T. Fujimoto, *Phys. Rev. E* **49**, 5565 (1994).
- [6] Fujimoto, *Plasma Spectroscopy* (The International Series of Monographs on Physics, 123, Oxford University Press, 2004).
- [7] R. Celiberto, R.K. Janev, A. Laricchiuta, M. Capitelli, J.M. Wadehra and D.E. Atems, *At. Data Nucl. Data Tables* **77**, 161 (2001).
- [8] K. Sawada, H. Nakamura, S. Saito, G. Kawamura, M. Kobayashi, K. Haga, R. Migita, T. Sawada and M. Hasuo, *Contrib. Plasma Phys.* e201900153 (2020).
- [9] S. Saito, H. Nakamura, K. Sawada, G. Kawamura, M. Kobayashi and M. Hasuo, *Contrib. Plasma Phys.* e201900152 (2020).